Design and Analysis of Heterogeneous Physical Layer Network Coding

Haoyuan Zhang, *Student Member, IEEE*, Lei Zheng, *Student Member, IEEE*, and Lin Cai, *Senior Member, IEEE*

***Abstract*—In this paper, physical layer network coding with heterogeneous modulations (HePNC) is proposed for the asymmetric two-way relay channel (TWRC) scenario. The existing PNC solutions using the same modulation for signals transmitted from two source nodes may not be desirable for practical situations when traffic loads exchanged between the sources are unequal and channel conditions of source-relay links are heterogeneous. HePNC includes two stages: multiple access (MA) and broadcast (BC) stages. In the MA stage, the two source nodes transmit to the relay simultaneously with heterogeneous modulations selected according to the channel conditions and the ratio of traffic loads exchanged between the sources, and then the signals superimposed at the relay are mapped to a network-coded symbol by a mapping function adaptively; in the BC stage, the relay broadcasts the network-coded symbol back to both sources with a modulation selected according to the bottleneck link's channel condition. We present three HePNC designs, including QPSK-BPSK, 8PSK-BPSK and 16QAM-BPSK HePNC. How to design and optimize the mapping function is investigated and the error performance of QPSK-BPSK HePNC is analyzed. We further study the HePNC system performance, throughput upper bound and energy efficiency. Extensive simulations demonstrated that the proposed HePNC can substantially enhance the throughput and energy efficiency compared with the existing PNC.**

I. Introduction

PHYSICAL layer network coding (PNC) was proposed in 2006 by Zhang *et al*. [2] and Popovski *et al*. [3], independently. The researches on PNC mainly focus on the two-way relay channel (TWRC) scenario, where two source nodes exchange information with the help of a relay, as they cannot reliably communicate with each other directly. With PNC, two source nodes transmit simultaneously towards a relay, where superimposed signals can be mapped and relayed instead of being treated as interference, so concurrent transmissions to the relay node result in a higher spectrum efficiency.

Most of the existing PNC designs are studied in a symmetric TWRC scenario, where the two source nodes use the same modulation for their signals. Although PNC can boost the system throughput substantially [2], using homogeneous modulation becomes inefficient in an asymmetric TWRC scenario where the two source-relay links have asymmetric channel conditions or the two source nodes have different amount of data to exchange. The heterogeneity in the asymmetric TWRC motivates us to develop a heterogeneous PNC scheme (HePNC) where the sources use heterogeneous modulations.

Similar to the traditional PNC, the HePNC procedure has two stages: multiple access (MA) stage and broadcast (BC) stage. In the MA stage, the relay receives the superimposed signals transmitted simultaneously from the sources, and then maps the received signals to a network-coded symbol by a mapping function. The mapping function is a critical issue in the PNC design. In the original design of PNC in [2], XOR mapping was adopted. However, with different channel conditions of the two source-relay links, the amplitude attenuations and phase shifts of the two received signals from the sources are different, which directly influences the received constellation map at the relay, and further affects the demodulation success rate and system performance. Thus, adapting the mapping function according to the channel conditions is necessary, which is known as adaptive mapping [4]. Mapping function design needs to satisfy the Latin square constraint [4], [5], which is a fundamental criterion to ensure that the network-coded symbol is decodable at the sources. One difference of HePNC and PNC is how to design and optimize the mapping function. In HePNC, adaptive mapping functions should be designed and optimized jointly considering the channel conditions, the Latin square constraint and the combination of different modulations.

The main contributions of this paper are four-fold. First, we propose the HePNC scheme in asymmetric TWRC, which enhances the communication efficiency of PNC in scenarios with asymmetric source-relay channel conditions and unequal traffic loads from the sources. Second, we present HePNC sample designs, including QPSK-BPSK, 8PSK-BPSK and 16QAM-BPSK HePNC. The design and optimization of the mapping functions following the Latin square constraint are investigated and presented. Third, we develop an analytical framework to derive the error performance of QPSK-BPSK HePNC under AWGN channels, and its performance bound under Rayleigh fading channels. Fourth, we evaluate the HePNC system performance in an asymmetric TWRC scenario. The throughput upper bound and energy efficiency with different ratios of traffic loads of the two sources are further discussed.

The rest of this paper is organized as follows. Related work are summarized in Sec. II. Sec. III introduces the system model and HePNC procedure in an asymmetric TWRC scenario. In Sec. IV, we elaborate the design criterion of QPSK-BPSK HePNC, and further discuss higher-order modulation

Manuscript received January 1, 2015; revised June 4, 2015 and September 8, 2015; accepted November 11, 2015. Date of publication December 1, 2015; date of current version April 7, 2016. This work has been presented in the IEEE Globecom, Austin, America, December 2014 [1]. The associate editor coordinating the review of this paper and approving it for publication was S. C. Liew.

The authors are with the Department of Electrical and Computer Engineering, University of Victoria, Victoria, BC V8W 3P6, Canada (e-mail: hyuan@uvic.ca; zhengl@uvic.ca; cai@uvic.ca).

Color versions of one or more of the figures in this paper are available online at http://ieeexplore.ieee.org.

Digital Object Identifier 10.1109/TWC.2015.2504471

HePNC. Sec. V analyzes the error performance of QPSK-BPSK HePNC. Simulation results are presented in Sec. VI, followed by concluding remarks in Sec. VII.

II. Related Work

PNC [2], [3] extends the operation of network coding [6], [7] in the PHY layer, and a comprehensive survey of PNC can be found in [8]. Two key issues in PNC system are how to design the mapping function and how to represent the network-coded symbol to guarantee that the sources can abstract each other's information accurately and effectively. In dynamic mapping function design, i.e., adaptive mapping [4], mapping function's selection varies with the channel conditions, which benefits the system performance at the cost of higher complexity and overheads. According to whether the network-coded symbol is represented by a finite field or an infinite field [9], generally PNC can be classified as finite-field PNC [4], [10] and infinite-field PNC [11]–[14]. Infinite-field PNC benefits from the simplicity to implement, while the performance is affected by the amplified and forwarded noise. Finite-field PNC tries to remove the noise at the relay and can achieve near information-capacity rates [15], [16]. Our work focuses on the dynamic mapping function design in the finite-field PNC.

In the literature, PNC is mainly investigated in a symmetric TWRC scenario, where the channel conditions of the two source-relay links are similar, and the sources select the same coding and modulation [4], [11]–[14], [17]–[23]. When the channel conditions of the two source-relay links are quite different, the scenario is specified as asymmetric TWRC. In [24], the impact of the asymmetric channels on PNC was studied, where both sources still use the BPSK modulation. Sources can also select different modulations according to the channel conditions in asymmetric TWRC [25]–[27]. In [25], adaptive modulation and network coding (AMNC) was proposed. Sources select modulations according to the amplitude ratio of the two source-relay channel gains, however, the influence of the random phase shift difference was not addressed. [26], [27] focused on how to design the network-coded symbol at the relay. Consider 2^{q_1}-ary and 2^{q_2}-ary constellations for the two sources' signals, respectively. In [26], decode-and-forward joint-modulation (DF-JM) was proposed, where the network-coded symbol was represented by a $2^{q_1+q_2}$-ary constellation, which is composed of the direct combinations of the two source symbols. In [27], two joint modulation and relaying solutions were proposed, JMR1 (a variant of DF-JM) and JMR2. In JMR2, the relay uses a many-to-one mapping function to obtain a $2^{\max(q_1,q_2)}$-ary network-coded symbol, while the impact of the phase shift difference between the superimposed symbols at the relay was not addressed. In [4], a method to design the many-to-one mapping function known as adaptive mapping was proposed for symmetric TWRC, where the relay can design and select different many-to-one functions according to the channel conditions. The many-to-one mapping design should follow the Latin square constraint [5], also known as the exclusive law [4].

In this paper, we propose HePNC and investigate how to design and optimize the mapping function and the network-coded symbol by jointly considering the channel conditions, the Latin square constraint and the combination of heterogeneous modulations with a random phase shift between the two received signals at the relay in an asymmetric TWRC scenario. The proposed HePNC design is within the compute-and-forward (CF) framework, which was proposed in [28] and was extended in [29], [30] with the lattice network coding schemes, from the information theoretic perspective. [31], [32] followed the CF framework, where the pulse amplitude modulation (PAM) was considered and linear mapping functions were designed. Different from [31], [32], PSK/QAM modulations are considered in this paper, and the relay computes the channel conditions of the two source-relay links and maps the estimated sources' symbols with the designed mapping functions, which may or may not be linear.

III. HePNC in Asymmetric TWRC

A. System Model

Consider an asymmetric TWRC scenario, where the source nodes Alice and Bob exchange information through a relay, Ron, because the source nodes are out of each other's transmission range. Each node equips with one antenna[1]. We consider a block fading channel, and the channel conditions of the link Alice–Ron, L_{ar}, and that of the link Bob–Ron, L_{br}, are different. Without loss of generality, we assume that L_{ar} is better than L_{br}, and L_{ar} can support a higher-order modulation. We assume a symbol-level synchronization at the relay and perfect channel estimations at the receivers, i.e., the relay node in the MA stage and the source nodes in the BC stage. Synchronization problems in multi-hop networks have been extensively studied [34]. The feasibility study for the symbol-level synchronization can be found in [35]–[37]. Note that in HePNC, the carrier-phase synchronization is not required at the relay and the global full CSI is not required at the transmitters.

Similar to the traditional PNC, the HePNC procedure has two stages: the MA and BC stages. In the MA stage, the two source nodes transmit the signals to Ron simultaneously, and Ron demodulates and maps the received superimposed signals to a network-coded symbol. In the BC stage, the network-coded symbol is broadcasted back to the source nodes. Different from PNC, heterogeneous modulations can be selected by the sources according to L_{ar} and L_{br} in the MA stage, and more transmission slots may be needed to broadcast the network-coded symbol in the BC stage due to the bottleneck link L_{br}. We also consider that the data loads exchanged between the sources may be unequal. Throughout this paper, the HePNC design is only considered in a symbol-level manner, and we assume that the error coding is orthogonal to modulation and not considered in this work. How to combine error coding and modulation together remains a further research issue that is beyond the scope of this work.

B. HePNC Procedure

Let $\mathcal{M}_m$ be 2^m-PSK modulation with the modulation order of m and $\mathbb{Z}_{2^m}$ be a non-negative integer set, which denotes the

[1] An extension of HePNC to multiple-antenna scenario can be found in [33].

finite set with unity energy E_s and Gray constellation mapping, $\mathbb{Z}_{2^m}=\{0,1,\ldots,2^m-1\}$. Assume that S_a and S_b are the source symbols to be exchanged. Denote m_a and m_b as the modulation orders for Alice and Bob, respectively. Thus, we have $S_a \in \mathbb{Z}_{2^{m_a}}$, $S_b \in \mathbb{Z}_{2^{m_b}}$ and $m_a > m_b$.

1) Multiple Access (MA) Stage: In the MA stage, the received signal at Ron, Y_r can be expressed as

$$Y_r = H_a \mathcal{M}_{m_a}(S_a) + H_b \mathcal{M}_{m_b}(S_b) + N_r, \tag{1}$$

where H_a and H_b are the channel gains of L_{ar} and L_{br}, respectively, and N_r is the complex Gaussian noise with a variance of σ^2. Denote $H_b/H_a = \gamma \exp(j\theta)$, where γ and θ stand for the amplitude ratio and the phase difference of the two received signals, respectively. γ denotes the degree of asymmetry for the channel conditions of L_{ar} and L_{br}.

Define (S_a, S_b) as a symbol pair, which denotes the two sources' symbols S_a and S_b superimposed at Ron. The symbol pair (S_a, S_b) can also be represented by one constellation point on the received constellation map at Ron. The maximum likelihood (ML) detection is proceeded by Ron to jointly demodulate (S_a, S_b) from Y_r, and we have

$$(\hat{S}_a, \hat{S}_b) = \underset{(s_1,s_2)\in\mathbb{Z}_{2^{m_a}}\times\mathbb{Z}_{2^{m_b}}}{\operatorname{argmin}} \left|Y_r - H_a\mathcal{M}_{m_a}(s_1) - H_b\mathcal{M}_{m_b}(s_2)\right|^2, \tag{2}$$

where $(\hat{S}_a, \hat{S}_b)$ is the estimation of (S_a, S_b).

Afterwards, Ron uses a mapping function $\mathcal{C}$ to map $(\hat{S}_a, \hat{S}_b)$ to a network-coded symbol $S_r = \mathcal{C}(\hat{S}_a, \hat{S}_b)$, $S_r \in \mathbb{Z}_{2^{m_a}}$. The mapping function $\mathcal{C}$ applied by Ron is known by all nodes, and it subjects to the Latin square constraint [5] (also known as the exclusive law [4]), which requires

$$\begin{aligned} &\mathcal{C}(s_1, s_2) \neq \mathcal{C}(s_1', s_2) \text{ for any } s_1 \neq s_1' \in \mathbb{Z}_{2^{m_a}} \text{ and } s_2 \in \mathbb{Z}_{2^{m_b}}, \\ &\mathcal{C}(s_1, s_2) \neq \mathcal{C}(s_1, s_2') \text{ for any } s_2 \neq s_2' \in \mathbb{Z}_{2^{m_b}} \text{ and } s_1 \in \mathbb{Z}_{2^{m_a}}. \end{aligned} \tag{3}$$

Although the superimposed signals at Ron is $2^{(m_a \times m_b)}$-ary, the mapping function $\mathcal{C}$ can decrease the network-coded symbol to be 2^{m_a}-ary. The process of mapping $(\hat{S}_a, \hat{S}_b)$ to symbol S_r includes two steps, the many-to-one mapping step and the *relay labeling* step. The details of the many-to-one mapping and *relay labeling* will be given in Sec. IV-A and Sec. IV-B, respectively.

2) Broadcast (BC) Stage: Subjecting to the bottleneck link L_{br}, which can only support a lower-order modulation 2^{m_b}. The relay reduces the modulation order of the network-coded symbol S_r from m_a to m_b to guarantee the reliable transmission in the BC stage. Thus, HePNC applies a multiple-slots scheme to broadcast the network-coded symbol in the BC stage. Ron uses modulation $\mathcal{M}_{m_b}$ to broadcast S_r back to the source nodes by $\lceil \frac{m_a}{m_b} \rceil$ transmission slots in the BC stage[2]. In each transmission slot, a part of S_r denoted by $S_r' \in \mathbb{Z}_{2^{m_b}}$ is transmitted. An estimation of S_r is conducted at each source node by concatenating all the estimated S_r'. We use an example to explain the motivation of the multiple-slot design in the BC stage. Considering QPSK-BPSK HePNC, in order to ensure the bit error rate from the relay to Bob to be below 10^{-3} in the BC stage, the bottleneck link L_{br} with $\text{SNR}_{br} = 7\text{dB}$ can only support BPSK. The network-coded symbol S_r is a QPSK symbol, and thus, the relay uses two BC slots to broadcast one BPSK symbol in each BC slot to guarantee the BER threshold. Throughout this paper, SNR is defined as the received SNR. For Gaussian channels, it can be calculated by $\text{SNR(dB)} = 10\log_{10}\frac{E_r}{N_0}$, where E_r denotes the received symbol energy, and N_0 is the noise spectral density. For fading channels, SNR denotes the average received SNR.

For each transmission slot in the BC stage, Alice receives $Y_a = H_a\mathcal{M}_{m_b}(S_r') + N_a$ from Ron, where N_a is the complex Gaussian noise with a variance of σ^2. Alice estimates S_r' as $\hat{S}_r'$ by the ML decision

$$\hat{S}_r' = \underset{s_r'\in\mathbb{Z}_{2^{m_b}}}{\operatorname{argmin}} |Y_a - H_a\mathcal{M}_{m_b}(s_r')|^2. \tag{4}$$

Then, an estimation of S_r denoted as $\hat{S}_r$ is obtained by concatenating all the $\hat{S}_r'$. Finally, Alice estimates S_b by

$$\hat{S}_b' = \underset{s_b\in\mathbb{Z}_{2^{m_b}}}{\operatorname{argmin}} |\hat{S}_r - \mathcal{C}(S_a,\ s_b)|^2. \tag{5}$$

Note that in (5), Alice decodes Bob's information by using both the original information transmitted by itself in the MA stage and the mapping function $\mathcal{C}$. Similarly, Bob obtains the estimation of S_a.

C. QPSK-BPSK HePNC Example

Fig. 1 shows a sample design of QPSK-BPSK HePNC. Fig. 1(a) shows the QPSK-BPSK HePNC procedure literally, and Fig. 1(b) considers the procedure from the constellation map point of view. In the MA stage, Alice uses QPSK to send symbol $S_a = 1$ to Ron, meanwhile Bob uses BPSK to send $S_b = 0$ to Ron. Note that the QPSK symbol $S_a = 1$ can also be represented as '01' by two binary bits. In this paper, we use '.' scheme to present the binary bits that compose one symbol. The bit-symbol labeling method applied for QPSK constellation is shown in Fig. 1(b). Ron demodulates the symbol pair $(S_a, S_b) = (1, 0)$, and then uses a mapping function $\mathcal{C}$ as shown in Fig. 1(b) to obtain a network-coded symbol $S_r = \mathcal{C}(1, 0) = 1$, which can be represented by binary bits '01'. Since the bottleneck link L_{br} can only support BPSK, S_r is split into two BPSK symbols, 0 and 1, and broadcasted back by two transmission slots in the BC stage. After receiving S_r, Alice and Bob can decode each other's information with the same mapping function $\mathcal{C}$ and the original symbol transmitted by itself in the MA stage.

Fig. 1(b) shows the constellation maps at the sources and relay. In the received constellation map at Ron, the four dotted circles are composed of the expected received BPSK symbols $-H_b\exp(j\theta)$ and $H_b\exp(j\theta)$ with the phase difference θ and superimposing on the expected received QPSK symbol $H_a\mathcal{M}_2(S_a)$. We specify the circles as BPSK circles. Each center of the BPSK circles is the expected received QPSK symbol $H_a\mathcal{M}_2(S_a)$, and the radius of each BPSK circle equals H_b. We observe that, the structure of the received constellation map is

[2]If $\frac{m_a}{m_b}$ is not an integer, Ron can schedule several BC stages to transmit the least common multiple of m_a and m_b bits.

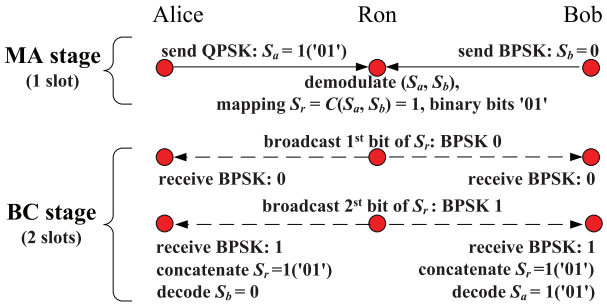

(a) MA and BC Stages for QPSK-BPSK HePNC.

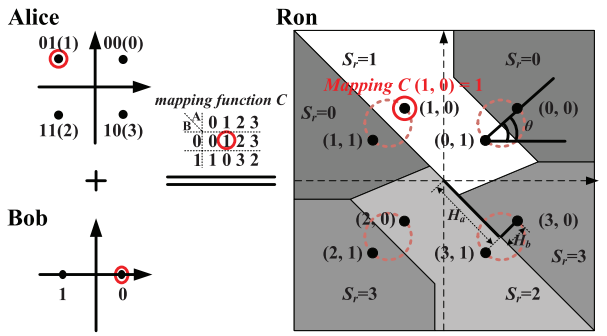

(b) Constellation maps at sources and relay with $\gamma = 0.3$ and $\theta = \frac{\pi}{4}$, the colored blocks represent the decision regions for the ML decision in (2) and the mapping results of S_r.

Fig. 1. An example of QPSK-BPSK HePNC.

determined by parameters γ and θ, and the size of the received constellation maps is determined by both H_a and H_b, which is a useful conclusion for designing the mapping function $\mathcal{C}$ discussed in the following section.

IV. HePNC Design and Analysis

A critical issue of HePNC is the mapping function $\mathcal{C}$ design including the many-to-one mapping $\mathcal{F}$ design and *relay labeling* design. We begin with QPSK-BPSK HePNC as a sample design to elaborate the design criterion, which presents insights for designing higher-order modulation HePNC. Then we present and discuss the 8PSK-BPSK HePNC and 16QAM-BPSK HePNC designs.

A. Many-to-One Mapping Design

The many-to-one mapping $\mathcal{F}$ is a $2^{\min(m_a,m_b)}$-to-one mapping. One feature of this many-to-one mapping scheme is that the superimposed signals at the relay are reduced from $2^{m_a \times m_b}$-ary to $2^{\max(m_a,m_b)}$-ary. The second feature is that part of the demodulation errors in the process of obtaining $(\hat{S}_a, \hat{S}_b)$ can be corrected, e.g., considering the example in Fig. 1, we have $(S_a, S_b) = (1, 0)$, and even if Ron demodulates $(\hat{S}_a, \hat{S}_b) = (0, 1)$ by mistake, the many-to-one mapping result is still correct if $\mathcal{F}(0, 1) = \mathcal{F}(1, 0)$. We discuss how to design the many-to-one mapping in the following.

Define the error rate of $S_r \neq \mathcal{C}(S_a, S_b)$ as the relay mapping error rate (RER). RER is an important performance index, which determines whether the network-coded symbol is correctly obtained before the BC stage. More details of the RER error performance estimation for QPSK-BPSK HePNC is analyzed in Sec. V-A. A proper many-to-one mapping design aims to minimize RER under the Latin square constraint. The RER performance is dominated by the smallest Euclidean distance between two symbol pairs, e.g., the Euclidean distance between symbol pairs (1, 0) and (1, 1) as shown in Fig. 1(b). However, (1, 0) and (1, 1) cannot be grouped together, because they violate the Latin square constraint. Given γ and θ, the optimal many-to-one mapping can be obtained by the *Closest Neighbor Clustering* (CNC) algorithm [4], which selects the symbol pairs with the smallest Euclidean distance under the condition that these two symbol pairs satisfy the Latin square constraint. The influence of the two source-relay channel conditions on the received constellation map can be reflected by parameters γ and θ, and optimal many-to-one mapping varies with γ and θ. Ron can select the optimal many-to-one mapping according to the channel conditions referred to parameters γ and θ [4]. Although obtaining the optimal mapping functions by the CNC method is of high complexity [5], they can be done offline, so the approach is feasible as the relay only needs to store the designed optimal mapping functions and looks up the labeling tables.

The *Closest Neighbor Clustering* algorithm can determine the many-to-one mapping, e.g., for QPSK-BPSK HePNC, when $\theta \in (0, \frac{\pi}{4})$ and $\gamma < 0.5$[3], the optimal many-to-one mapping $\mathcal{F}_1$ can be expressed as

$$\begin{aligned} &\mathcal{F}_1(0, 0) = \mathcal{F}_1(1, 1),\ \mathcal{F}_1(0, 1) = \mathcal{F}_1(1, 0), \\ &\mathcal{F}_1(2, 0) = \mathcal{F}_1(3, 1),\ \mathcal{F}_1(2, 1) = \mathcal{F}_1(3, 0). \end{aligned} \tag{6}$$

How to label the many-to-one mapping results by $S_r \in \mathbb{Z}_{2^{m_a}}$ is defined as *relay labeling*, and it will be discussed in the following subsection.

B. Relay Labeling Design

First, we clarify the differences between the bit-symbol labeling at each source and the *relay labeling* at the relay. Throughout this paper, each source applies the Gray mapping as the bit-symbol labeling, e.g., the bit-symbol labeling for QPSK as shown in Fig. 1(b). The *relay labeling* aims to label the many-to-one mapping results as shown in (6), which can be labeled by four two-bit QPSK symbols, and in the following we target to design and optimize the *relay labeling*.

Even Ron can correctly obtains $S_r = \mathcal{C}(S_a, S_b)$ in the MA stage, the source nodes may not successfully decode each other's information if there are errors in the broadcast stage. The link from Ron to Bob L_{br}[4] is the bottleneck link in the BC stage, which limits the throughput of the BC stage. We can optimize the *relay labeling* process by maximizing the successful transmission bits under the condition that error happens in at most one transmission slot over link L_{br} in the BC stage. Note that if an error happens in any transmission slot over link

[3]The threshold $\gamma = 0.5$ will be explained in Sec. IV-C.

[4]We denote both links from Bob to Ron and from Ron to Bob as L_{br}; however, the channel conditions can be different for the transmission from Bob to Ron in the MA stage and that from Ron to Bob in the BC stage.

TABLE I
SINGULAR FADE STATE POINTS OF QPSK-BPSK HEPNC

SFS points	P_1	P_2	P_3	P_4	P_5
γ,θ	$\frac{\sqrt{2}}{2}$, 0 or π	$\frac{\sqrt{2}}{2}$, $\frac{\pi}{2}$ or $\frac{3\pi}{2}$	$\frac{\sqrt{2}}{2}$, 0 or π	$\frac{\sqrt{2}}{2}$, $\frac{\pi}{2}$ or $\frac{3\pi}{2}$	1, $\frac{\pi}{4}$ or $\frac{3\pi}{4}$ or $\frac{5\pi}{4}$ or $\frac{7\pi}{4}$

TABLE II
DETAILS OF THE OPTIMAL MAPPING FUNCTIONS FOR QPSK-BPSK HEPNC

	0	1	2	3
0	0	1	2	3
1($\mathcal{C}_1$)	1	0	3	2
1($\mathcal{C}_2$)	3	2	1	0
1($\mathcal{C}_3$)	2	3	0	1

L_{ar} in the BC stage[5], source A cannot successfully decode the information from source B.

We use an example to illustrate the design criterion of the *relay labeling*. Consider the the QPSK-BPSK HePNC example as shown in Fig. 1, where the source symbols pair $(S_a, S_b) = (1, 0)$, which can also be expressed by as (S_a, S_b) =('01', 0) with the Gray mapping as shown in Fig. 1(b). Considering the many-to-one mapping $\mathcal{F}_1$ in (6) and supposing that $(\hat{S}_a, \hat{S}_b)$ are correctly estimated by Ron in the MA stage. Considering a worst case example of a random relay labeling, e.g., relay labels $\mathcal{F}_1(1, 0) = \mathcal{F}_1(0, 1)$ to be '00', $\mathcal{F}_1(3, 0) = \mathcal{F}_1(2, 1)$ to be '01', and then $S_r = \mathcal{F}_1(1, 0)$ is labeled to be '00' in bits. In the BC stage, when error happens in the second transmission slot over link L_{br}, Bob estimates the network-coded symbol to be $\hat{S}_r$ ='01' in error, and Bob finally decodes $\hat{S}'_a = 3$ in QPSK symbol, i.e., '10' in bits, by contrasting the mapping function $\mathcal{F}_1(3, 0)$. Thus, two bits are in error by decoding the expected S_a ='01' to be $\hat{S}'_a$='10'. When $S_b = 0$, one way to reduce the probability of the worst case is to label $\mathcal{F}_1(1, 0)$ and $\mathcal{F}_1(3, 0)$ according to Gray mapping, e.g., label $\mathcal{F}_1(1, 0)$ and $\mathcal{F}_1(3, 0)$ to be '01' and '10', respectively, and the same strategy is applied for $\mathcal{F}_1(0, 0)$ and $\mathcal{F}_1(2, 0)$, i.e., label $\mathcal{F}_1(0, 0)$ and $\mathcal{F}_1(2, 0)$ to be '00' and '11'. In this way, the worst case, i.e., two bits in error in the above example, only occurs when errors happen in both of the L_{br} transmissions.

The labeling design that only considers the case $S_b = 0$ may not be suitable for the case $S_b = 1$, so the *relay labeling* for $\mathcal{F}(s_a, 0)$ and $\mathcal{F}(s_a, 1)$ ($s_a \in \mathbb{Z}_4$) should be jointly optimized. With an exhaustive search, we find that for QPSK-BPSK HePNC, the optimal *relay labeling* can simply label $\mathcal{F}(s_a, 0) = s_a$, and then label $\mathcal{F}(s_a, 1)$ according to the selected many-to-one mapping $\mathcal{F}$. To generalize the bit-symbol labeling for QPSK-BPSK HePNC, there are three types of bit-symbol labeling for the QPSK modulation, please refer to Fig. 1 in [26], and with any type of QPSK bit-symbol labeling in QPSK-BPSK HePNC, the optimal relay labeling conclusion above is still valid. Note that the optimal *relay labeling* is not unique.

C. Mapping Function $\mathcal{C}$ of QPSK-BPSK HePNC

The mapping function $\mathcal{C}$ design includes the many-to-one mapping $\mathcal{F}$ design and the *relay labeling* design, which are analyzed in the above two subsections. Thus, the optimal mapping function for QPSK-BPSK HePNC can be designed and shown in Fig. 2, and the details of the many-to-one mapping and relay labeling are shown in Table II. Depending on the two source-relay channel conditions, i.e., γ and θ, the mapping functions can be adaptively selected by the relay according to Fig. 2. When γ is small, e.g., $\gamma \in (0, 0.5)$, the whole region is only divided into two parts labeled by $\mathcal{C}_1$ and $\mathcal{C}_2$; when $\gamma \in (0, 1)$[6], the whole region can be divided into three parts, labeled by mapping functions $\mathcal{C}_1$, $\mathcal{C}_2$ and $\mathcal{C}_3$, respectively. A general explanation is that with the increase of γ, the BPSK circles on the received constellation map at the relay as shown in Fig. 1(b) become larger, which changes the smallest Euclidean distance between constellation points with the shifting of θ, and thus $\mathcal{C}_3$ occurs when $\gamma \in (0.5, 1)$.

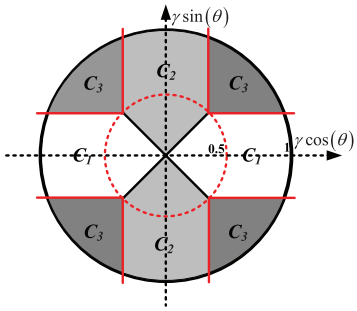

Fig. 2. QPSK-BPSK HePNC adaptive mapping functions.

Define η as the boundary of different adaptive mapping functions C_1, C_2 and C_3 when $\theta \in (0, \frac{\pi}{2})$ as shown in Fig. 2, and we have

$$\eta = \begin{cases} \dfrac{\pi}{4}, & \text{when } \gamma < 0.5; \\ \arcsin\dfrac{\sqrt{2}}{4\gamma}, & \text{when } 0.5 < \gamma < 1. \end{cases} \tag{7}$$

We use Fig. 3 to explain how to obtain (7), and the threshold $\gamma = 0.5$ is indirectly explained. When $\gamma < 0.5$, the received constellation at the relay is shown in Fig. 3(a). When $\theta \in (0, \frac{\pi}{4})$, the smallest Euclidean distance is that between (1,0) and (0,1), and also the distance between (2,0) and (3,1). Thus, (1,0) and (0,1) are mapped to the same cluster, and the same for (2,0) and (3,1). Then, we can obtain the mapping function $\mathcal{C}_1$. When $\theta = \frac{\pi}{4}$, the distance between (1,0) and (0,1) equals the distance between (0,1) and (3,0); when $\theta \in (\frac{\pi}{4}, \frac{\pi}{2})$, the smallest Euclidean distance is that between (1,1) and (2,0), and also the distance between (3,0) and (0,1), which results in mapping function $\mathcal{C}_2$. Thus, $\eta = \frac{\pi}{4}$ is the boundary of mapping functions $\mathcal{C}_1$ and $\mathcal{C}_2$ for $\gamma < 0.5$. Fig. 3(b) shows the received constellation map when $\gamma > 0.5$. We can see that, with the increase of θ from 0 to $\frac{\pi}{4}$, before $\theta = \frac{\pi}{4}$, these exists a θ where the

[5]As L_{ar} has a relatively better channel condition comparing to L_{br}, this error probability can be neglected at high SNR.

[6]We consider the asymmetric TWRC, and the channel condition of L_{ar} is better than that of L_{br}, and thus we have $\gamma \in (0, 1)$.

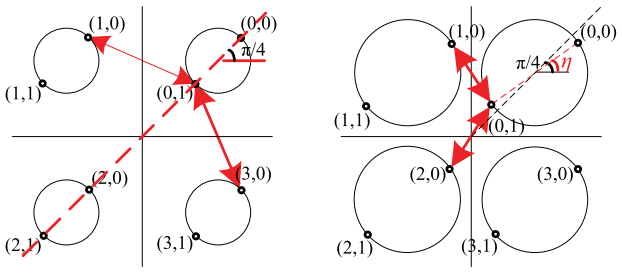

(a) $\gamma < 0.5$. (b) $\gamma > 0.5$.

Fig. 3. An example of the mapping function's boundary.

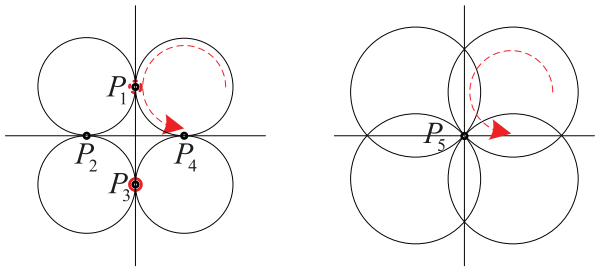

(a) $\gamma = \frac{\sqrt{2}}{2}$. (b) $\gamma = 1$.

Fig. 4. Singular fade state points of QPSK-BPSK HePNC constellations.

distance between (1,0) and (0,1) equals that between (0,1) and (2,0). This value of θ is the boundary, η, of the mapping functions $\mathcal{C}_1$ and $\mathcal{C}_3$. Note that with the increase of γ from 0 to 1, this situation happens first when $\gamma = 0.5$ and $\theta = \frac{\pi}{4}$, and thus $\gamma = 0.5$ is the threshold. By letting the Euclidean between (1,0) and (0,1) equal the distance between (0,1) and (2,0), we can easily obtain $\eta = \arcsin\frac{\sqrt{2}}{4\gamma}$. Another method to obtain the threshold $\gamma = 0.5$ is to let $\eta = \frac{\pi}{4}$, and then we have $\gamma = 0.5$ according to $\eta = \arcsin\frac{\sqrt{2}}{4\gamma}$, which indicates the situation that the first time $\mathcal{C}_3$ occurs with the increase of γ from 0 to 1.

The CNC method is applied to design the adaptive mapping functions in this paper, another well known mapping function design method targets to remove the singular fade state (SFS) of the received constellations at the relay [5]. SFS denotes the case when the minimum distance of the received constellation points at the relay becomes zero, which results in large error probabilities if without suitable mapping function designs. We use an example to show that the SFS points of QPSK-BPSK HePNC constellations at the relay can be removed by the designed mapping functions as shown in Fig. 2. For QPSK-BPSK HePNC, the SFS points on the received constellation map at the relay are shown in Fig. 4 and summarized in Table I, labeled from P_1 to P_5[7]. The SFS points P_1 and P_3 can be removed by mapping function $\mathcal{C}_1$, and P_2 and P_4 can be removed by $\mathcal{C}_2$, and P_5 can be removed by $\mathcal{C}_3$. For example, considering the case shown in Fig. 4(a), when $\gamma = \frac{\sqrt{2}}{2}$ and $\theta = 0$, symbol pairs (0,1) and (1,0) overlap on the received constellation resulting in the SFS point P_1, which is marked by the red dotted circle, and (2,0) and (3,1) overlap to be another SFS point P_3 marked by the red lined circle. By the mapping function $\mathcal{C}_1$, (0,1) and (1,0) are mapped to the same network-coded symbol, and the same for (2,0) and (3,1). Thus, P_1 and P_3 can be removed. The other SFS points can also be removed by the designed mapping functions similarly.

[7]Note that, $\gamma = 0$ and $\gamma = \infty$ can be considered as two special cases resulting in non-removable singular fade state points, which also exist in other PNC schemes.

TABLE III
DETAILS OF THE OPTIMAL MAPPING FUNCTIONS FOR 8PSK-BPSK HEPNC

	0	1	2	3	4	5	6	7
0	0	1	2	3	4	5	6	7
$1(\mathcal{C}_1)$	1	2	7	6	3	4	5	0
$1(\mathcal{C}_2)$	1	2	3	0	7	4	5	6
$1(\mathcal{C}_3)$	7	2	3	4	1	0	5	6
$1(\mathcal{C}_4)$	7	0	3	4	5	2	1	6
$1(\mathcal{C}_5)$	7	0	1	4	5	6	3	2
$1(\mathcal{C}_6)$	3	0	1	2	5	6	7	4
$1(\mathcal{C}_7)$	5	4	1	2	3	6	7	0
$1(\mathcal{C}_8)$	1	6	5	2	3	4	7	0
$1(\mathcal{C}_9)$	2	7	0	5	6	3	4	1
$1(\mathcal{C}_{10})$	6	3	4	1	2	7	0	5

In the MA stage, the relay obtains the two source-relay's channel conditions H_a and H_b by channel estimations, where H_a and H_b are complex numbers. By the definition $H_b/H_a = \gamma\exp(j\theta)$, γ and θ can be obtained. Then the relay can select the optimal mapping function $\mathcal{C}$ according to Fig. 2 referring to parameters γ and θ, and find the details of the mapping function $\mathcal{C}$ including the many-to-one mapping and relay labeling by Table II. For example, when $\gamma < 0.5$, $\theta \in (0, \frac{\pi}{4})$ and $(\frac{7\pi}{4}, 2\pi)$, the optimal mapping function $\mathcal{C}_1$ should be applied, and the details of the mapping function $\mathcal{C}_1$ can be found according to Table II, which is the same as the mapping function used in Fig. 1(b). If $\mathcal{C}_2$ or $\mathcal{C}_3$ is found to be optimal, the first row of the mapping function is not changed, i.e., $\mathcal{F}(s_a, 0) = s_a$, and only the second row is changed accordingly. Note that, the mapping functions $\mathcal{C}_1$ and $\mathcal{C}_2$ are non-linear, but $\mathcal{C}_3$ is linear [31]. In other words, HePNC can be possibly applied for both non-linear and linear PNC mapping. Please refer to [31] for more discussions about the optimization of the linear PNC design.

D. Further Discussion on Higher-Order Modulation HePNC

For other higher-order modulation HePNC, such as 8PSK-BPSK and 16QAM-BPSK HePNC, the optimal many-to-one mapping and *relay labeling* can also be obtained by the *Closest Neighbor Clustering* algorithm and exhaustive search as discussed above. However, as the set size of the superimposed signals increases for higher-order modulation HePNC, the number of the optimal mapping functions increases especially when γ is large, which increases the complexity of the mapping function selection and the relay needs to change the mapping function frequently.

Simplified mapping function $\mathcal{C}$ designs for 8PSK-BPSK and 16QAM-BPSK HePNC are shown in Figs. 5(a) and 5(b), respectively. Table III shows the details of the 8PSK-BPSK HePNC mapping function design. The mapping details of 16QAM-BPSK HePNC is omitted due to the space limit. The

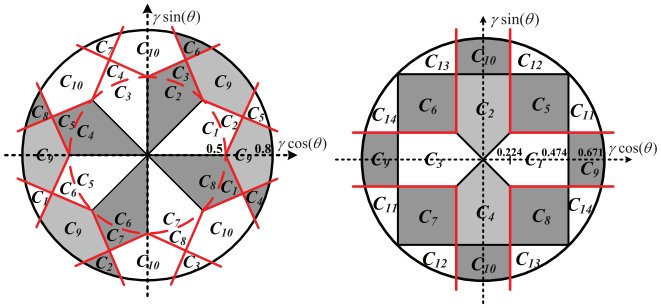

(a) 8PSK-BPSK HePNC. (b) 16QAM-BPSK HePNC.

Fig. 5. Mapping functions for 8PSK-BPSK and 16QAM-BPSK HePNC.

procedure of obtaining Fig. 5(a) and Table III is summarized as follows:

1) When $\gamma < 0.5$, obtain the optimal many-to-one mapping set $\mathcal{F} = \{\mathcal{F}_1, \cdots, \mathcal{F}_8\}$ by the *Closest Neighbor Clustering* algorithm.[8]
2) When $\gamma > 0.5$, given γ and θ, find all of the pairwise symbol pairs (s_1, s_2) and (s_1', s_2') satisfying the conditions that they have the smallest Euclidean distance and satisfy the Latin square constraint, i.e., $s_1 \neq s_1'$ and $s_2 \neq s_2'$. Note that several pairwise symbol pairs may satisfy the above two conditions.
3) Generate a temporary mapping way $\mathcal{F}_{temp}(s_1, s_2) = \mathcal{F}_{temp}(s_1', s_2')$, $\mathcal{F}_{temp}$ contains the mapping ways for all the pairwise symbol pairs obtained in step 2.
4) Check whether $\mathcal{F}_{temp}(s_1, s_2) = \mathcal{F}_{temp}(s_1', s_2')$ can be included by the existing many-to-one mapping in set $\mathcal{F}$.
5) If any many-to-one mapping $\mathcal{F}_i$ ($\mathcal{F}_i \in \mathcal{F}$) includes $\mathcal{F}_{temp}$, update $\mathcal{F}_{temp} = \mathcal{F}_i$; if none of the existing many-to-one mapping includes $\mathcal{F}_{temp}$, generate a new many-to-one mapping $\mathcal{F}_9$, update $\mathcal{F}_9 = F_{temp}$, and put $\mathcal{F}_9$ into set $\mathcal{F}$.
6) Repeat steps 2, 3, 4 and 5, and obtain all the many-to-one mapping $\mathcal{F} = \{\mathcal{F}_1, \cdots, \mathcal{F}_{10}\}$.[9]
7) For all $\mathcal{F} = \{\mathcal{F}_1, \cdots, \mathcal{F}_{10}\}$, label the mapping results by $\mathcal{F}(s_a, 0) = s_a$, label $\mathcal{F}(s_a, 1)$ according to the determined $\mathcal{F}$, and obtain mapping functions $\{\mathcal{C}_1, \cdots, \mathcal{C}_{10}\}$.

Similarly, the mapping functions for 16QAM-BPSK HePNC as shown in Fig. 5(b) can be obtained. For 8PSK-BPSK and 16QAM-BPSK HePNC, for all the many-to-one mappings, we can use exhaustive searching to find the optimal *relay labeling* $\mathcal{F}(s_a, 0) = s_a, s_a \in \mathbb{Z}_{2^{m_a}}$.

With the increase of γ, the size of BPSK circles would go larger, and the constellation points on the received constellation map at the relay can superimpose on each other which leads to more errors. Higher-order modulation HePNC can only be supported when γ is small enough. To initialize the HePNC transmission, and a HePNC scheme should be selected first according to the SNR of the two source-relay links and the data exchange ratio requirements, which is similar to the concept of adaptive modulation. In the initialization of HePNC, the source nodes report the requirements of the data amount needed to be exchanged individually, and then the relay estimates the two source-relay channel conditions and determines the modulations applied by the sources by jointly considering the two source-relay channel conditions and the data exchange requirements, and feedbacks the modulation configuration to the sources. Generally speaking, the source node who wants to exchange a larger amount of data should have a source-relay link with relatively better channel condition, which can be satisfied when an appropriate relay node is selected for the sources.

[8]The threshold $\gamma = 0.5$ for 8PSK-BPSK HePNC is obtained by exhaustive searching using the *Closest Neighbor Clustering* algorithm, and the theoretical proof is similar to that analyzed in Sec. IV-C to obtain the threshold $\gamma = 0.5$ for QPSK-BPSK HePNC.

[9]$\mathcal{F}_9$ and $\mathcal{F}_{10}$ are generated because they cannot be included by the existing many-to-one mapping in set $\mathcal{F}$.

V. Error Probability Analysis

In this section, we analyze the error performance of QPSK-BPSK HePNC[10]. We use the techniques introduced in [38]–[41] and calculate the error probabilities of RER and bit error rate (BER) of QPSK-BPSK HePNC under AWGN channels, and obtain a performance bound under Rayleigh fading channels.

A. Relay Mapping Error Analysis

We study the RER performance of the QPSK-BPSK HePNC system under AWGN channels first. The Rayleigh fading effect will be discussed in Sec. V-C. Denote the SNR for link L_{ar} and L_{br} as SNR_{ar} and SNR_{br}, respectively[11]. Denote $\Delta\text{SNR(dB)} = \text{SNR}_{ar}\text{(dB)} - \text{SNR}_{br}\text{(dB)}$. Considering path loss, the average received SNR of all links are inversely proportional to the link distance to the power of the path loss exponent α. By derivation, we have

$$\gamma = |H_b|/|H_a| = 10^{(-\Delta\text{SNR(dB)}/20)}. \tag{8}$$

Considering a complex plane, Fig. 6 shows the received constellation map at the relay and the decision boundaries for constellation point C when $\gamma \in (0, \frac{\sqrt{2}}{2})$ and $\theta \in (0, 2\pi)$. Note that C represents the symbol pair $(S_a, S_b) = (1, 0)$, which is also used in the example introduced in Fig. 1. For all $\gamma \in (0, \frac{\sqrt{2}}{2})$, BPSK circles always lie in each quadrant, and the decision boundaries as shown in Fig. 6 are always valid. When $\gamma > \frac{\sqrt{2}}{2}$, BPSK circles would cross X and Y axes; thus, new decision boundaries are needed. According to (8), when $\Delta\text{SNR} = 3$ dB, $\gamma \approx \frac{\sqrt{2}}{2}$, so $\gamma \in (0, \frac{\sqrt{2}}{2})$ covers the range $\Delta\text{SNR} \geq 3$ dB, which is suitable for QPSK-BPSK HePNC, as the SNR difference between QPSK and BPSK modulations to maintain a raw symbol error rate (SER) lower than 10^{-3} is about 3 dB.

Each symbol pair (S_a, S_b), $S_a \in \mathbb{Z}_4$ and $S_b \in \mathbb{Z}_2$, has the same transmitting probability $\frac{1}{8}$, and the expected received constellation map has the symmetric feature considering $\theta \in [0, 2\pi)$ with a uniform distribution. Thus, the RER performance can

[10]For higher-order modulation HePNC, the received constellation map at the relay contains more symbol pairs, i.e., $2^{m_1+m_2}$, which introduces more complexity to error performance analysis by the technique in [38]–[41].

[11]SNR denotes the numerical ratio of the received signal's power over the noise's power $2\sigma^2$, except the cases we specify the SNR in terms of (dB).

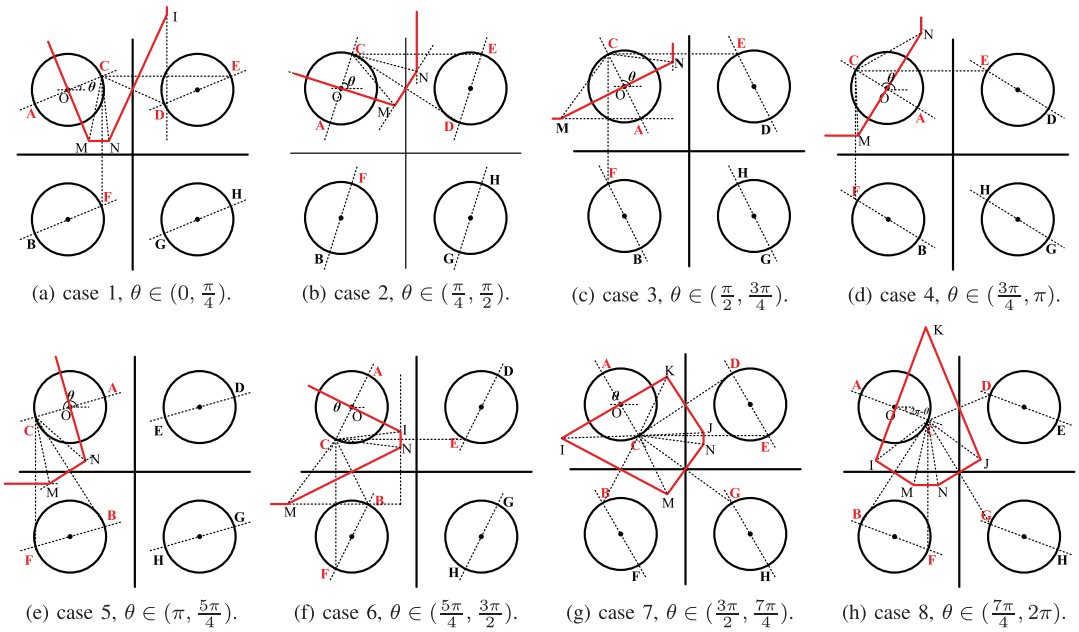

(a) case 1, $\theta \in (0, \frac{\pi}{4})$. (b) case 2, $\theta \in (\frac{\pi}{4}, \frac{\pi}{2})$. (c) case 3, $\theta \in (\frac{\pi}{2}, \frac{3\pi}{4})$. (d) case 4, $\theta \in (\frac{3\pi}{4}, \pi)$.

(e) case 5, $\theta \in (\pi, \frac{5\pi}{4})$. (f) case 6, $\theta \in (\frac{5\pi}{4}, \frac{3\pi}{2})$. (g) case 7, $\theta \in (\frac{3\pi}{2}, \frac{7\pi}{4})$. (h) case 8, $\theta \in (\frac{7\pi}{4}, 2\pi)$.

Fig. 6. Decision boundaries for $\gamma \in (0, \frac{\sqrt{2}}{2})$ and $\theta \in (0, 2\pi)$.

be calculated by only considering one symbol pair, e.g., the constellation point C. Then by calculating all $\theta \in [0, 2\pi)$, all the cases are considered. We use Fig. 6(a) as an example to illustrate. C is the expected received constellation point, and Ron may demodulate (S_a, S_b) as A, D, E and F falsely due to the noise. The coordinates of the constellation points from A to H are obtained by

$$H_a \mathcal{M}_{m_a}(s_1) + H_b \mathcal{M}_{m_b}(s_2), \text{ for all } s_1 \in \mathbb{Z}_4, \ s_2 \in \mathbb{Z}_2. \tag{9}$$

Points M, N and I are used for auxiliary calculation, so they are not the practical constellation points. The coordinates of points M, N and I are given by

$$\begin{cases} M = [-H_b \frac{\sin^2(\theta)}{\cos(\theta)} + \frac{\sqrt{2}}{2} H_a (\frac{\sin(\theta)}{\cos(\theta)} - 1)] + j[H_b \sin(\theta)], \\ N = [-H_b \sin(\theta)] + j[H_b \sin(\theta)], \\ I = [H_b \cos(\theta)] + j[\frac{\sqrt{2}}{2} H_a (\frac{\sin(\theta)}{\cos(\theta)} + 1) - H_b \frac{\cos^2(\theta)}{\sin(\theta)}]. \end{cases}$$

Denote the error probability of mapping the desired constellation x_1 to the error constellation point x_2 as $P_{x_1 x_2}$, and denote the Euclidean distance between x_1 and x_2 as $D_{x_1 x_2}$. We obtain the error probabilities by

$$\begin{cases} P_{CA} = \frac{1}{2\pi} \int_0^{\angle ACM + \frac{\pi}{2}} \exp(\frac{-(D_{CA}/2)^2}{2\sigma^2 \sin^2(\theta')}) \mathrm{d}\theta', \\ P_{CF} = \frac{1}{2\pi} \int_0^{\angle MCN} \exp(\frac{-(D_{CF}/2)^2}{2\sigma^2 \sin^2(\theta' + \angle CMN)}) \mathrm{d}\theta', \\ P_{CD} = \frac{1}{2\pi} \int_0^{\angle NCI} \exp(\frac{-(D_{CD}/2)^2}{2\sigma^2 \sin^2(\theta' + \angle CNI)}) \mathrm{d}\theta', \\ P_{CE} = \frac{1}{2\pi} \int_0^{\frac{\pi}{2} - \angle ICE} \exp(\frac{-(D_{CE}/2)^2}{2\sigma^2 \sin^2(\theta' + \frac{\pi}{2} + \angle ICE)}) \mathrm{d}\theta'. \end{cases}$$

The RER calculation also needs to consider the positive influence of the adaptive mapping functions, as partial demodulation errors can be corrected by the many-to-one mapping scheme discussed in Sec. IV-A. Errors of P_{CD}, P_{CB} and P_{CG} can be corrected by the mapping functions $\mathcal{C}_1$, $\mathcal{C}_2$ and $\mathcal{C}_3$, respectively.

Denote RER_i, $i \in \{1, \cdots, 8\}$, as the relay mapping error for case i. RER_1 can be calculated by

$$\mathrm{RER}_1 = \frac{1}{2\pi} [\int_{\theta \in (0, \frac{\pi}{4})} (P_{CA} + P_{CF} + P_{CE}) \, \mathrm{d}\theta + \int_{\theta \in (\frac{\pi}{4} - \eta, \frac{\pi}{4})} P_{CD} \, \mathrm{d}\theta]. \tag{10}$$

Summing all RER_i obtains the overall $\mathrm{RER} = \sum_{i=1}^{8} \mathrm{RER}_i$. Note that for different RER_i, the decision boundaries and adaptive mapping functions should be jointly considered.

The error probability of P_{CA} exists in all RER_i, and P_{CA} indicates the rate of errors happened within the BPSK circle, which is

$$P_{CA} = \Pr\{S_r = C(S_a, 1 - S_b)\}. \tag{11}$$

When $\gamma \in (0, \frac{\sqrt{2}}{2})$, $D_{CA} = |H_b|$ is always the smallest Euclidean distance between the two symbols in the received constellation map that contributes to most errors, as other symbol errors due to smaller symbol Euclidean distances than D_{CA} can be corrected by the adaptive mapping function $\mathcal{C}$. Thus, according to the minimum distance criterion, the overall RER can be estimated by only considering the error probability $P_{CA} = Q[\frac{H_b}{\sigma}] = Q[\sqrt{2 \cdot \mathrm{SNR}_{br}}]$ when γ is small enough, where $Q[.]$ is the Q function.

B. System End-to-End BER Analysis

Denote BER_{ab} and BER_{ba} as the end-to-end BER from Alice to Bob and Bob to Alice, respectively. Denote BER_{all} as the overall BER. For QPSK-BPSK HePNC, we have $\mathrm{BER}_{all} = (2 \cdot \mathrm{BER}_{ab} + \mathrm{BER}_{ba})/3$.

For simplicity, let $\alpha_1 = (1 - Q[\sqrt{2 \cdot \mathrm{SNR}_{ar}}])^2$ and $\alpha_2 = (1 - Q[\sqrt{2 \cdot \mathrm{SNR}_{br}}])^2$, which denote the probabilities that there is no error in the transmissions over L_{ar} and L_{br} respectively in the BC stage. The probability that Ron obtains a

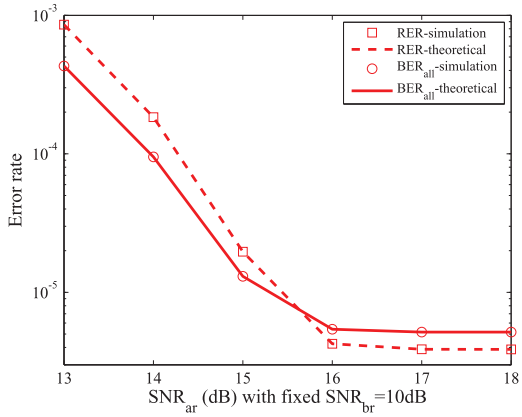

Fig. 7. Simulation and theoretical results under AWGN channels.

correct network-coded symbol $S_r = \mathcal{C}(S_a, S_b)$ equals 1-RER. If $S_r \neq \mathcal{C}(S_a, S_b)$, it is counted as an error event. BER_{ba} and BER_{ab} can be estimated by

$$\text{BER}_{ba} \approx \begin{cases} (1-\text{RER})(1-\alpha_1), & \text{when} S_r = \mathcal{C}(S_a, S_b), \\ \text{RER}, & \text{when} S_r \neq \mathcal{C}(S_a, S_b), \end{cases} \tag{12}$$

$$\text{BER}_{ab} \approx \begin{cases} (1-\text{RER})(1-\alpha_2)/2, & \text{when} S_r = \mathcal{C}(S_a, S_b), \\ \text{RER}/2, & \text{when} S_r \neq \mathcal{C}(S_a, S_b) \end{cases}. \tag{13}$$

Then we can estimate BER_{all} by

$$\text{BER}_{all} \approx \frac{2 \cdot \text{RER} + 2 \cdot Q[\sqrt{2 \cdot \text{SNR}_{br}}]}{3}. \tag{14}$$

Note that in (13), when $S_r = \mathcal{C}(S_a, S_b)$, we apply the conclusion from the *relay labeling* design, i.e., Bob can still successfully receive one bit from Alice if an error happens in any of the two transmissions over L_{br} in the BC stage. Fig. 7 shows the theoretical and simulation results for QPSK-BPSK HePNC under AWGN channels, with fixed $\text{SNR}_{br} = 10$ dB. When SNR_{ar} is small, the BPSK circles are relatively large which leads to a larger RER; when SNR_{ar} is large, the RER performance is mainly determined by $Q[\sqrt{2 \cdot \text{SNR}_{br}}]$, and the errors that happen in the bottleneck link L_{br} dominate the performance of the BC stage.

C. Rayleigh Fading Channels

We analyze the RER performance under the Rayleigh fading channels in this subsection. Denote the probability density function (PDF) of Rayleigh distribution as $f(x, \delta) = \frac{x}{\delta^2} \exp(\frac{-x^2}{2\delta^2})$, with the mean $E(x) = \delta\sqrt{\frac{\pi}{2}}$. Denote the PDF of channel gains H_a and H_b as $f(H_a, \delta_2)$ and $f(H_b, \delta_1)$, respectively. The PDF of γ can be calculated by

$$\text{PDF}(\gamma) = \int_0^\infty H_a f(H_a\gamma, \delta_1) \text{d}H_a = \frac{2\gamma {\delta_1}^2 {\delta_2}^2}{({\delta_1}^2 + {\delta_2}^2\gamma^2)^2}. \tag{15}$$

The $\text{PDF}(\gamma)$ and the cumulative distribution function (CDF) of γ, $\text{CDF}(\gamma)$, are shown in Fig. 8. When ΔSNR is large,

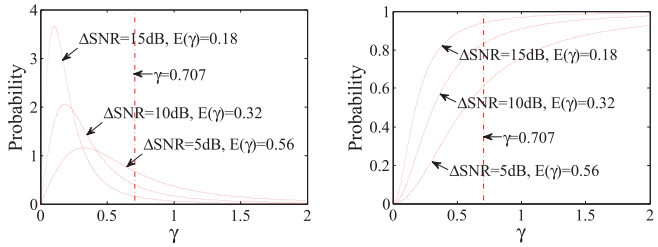

(a) PDF(γ). (b) CDF(γ).

Fig. 8. PDF and CDF of γ.

γ is within the range of $(0, \frac{\sqrt{2}}{2})$ with a higher probability, e.g., when $\Delta\text{SNR} = 15$ dB, $\text{CDF}(\gamma = \frac{\sqrt{2}}{2})$=94.04%. We can conclude that, in the Rayleigh fading channels, the RER of QPSK-BPSK HePNC is upper bounded by

$$\int_0^\infty f(H_b, \delta_2) Q\left[\frac{H_b}{\sigma}\right] \text{d}H_b, \tag{16}$$

which is derived as follows. Under the Rayleigh fading channels, RER can be expressed as

$$\int_0^\infty \int_0^\infty f(H_b, \delta_2) \text{PDF}(\gamma) f_{rer}(H_b, \gamma) \text{d}H_b \text{d}\gamma,$$

where $f_{rer}(H_b, \gamma)$ denotes the RER expression related to parameters H_b and γ. When $\gamma \in (0, \frac{\sqrt{2}}{2})$, with the minimum distance criterion and the analysis for (11), we have

$$\int_0^\infty \int_0^{\sqrt{2}/2} f(H_b, \delta_2) \text{PDF}(\gamma) Q\left[\frac{H_b}{\sigma}\right] \text{d}H_b \text{d}\gamma < \text{RER};$$

when $\gamma > \frac{\sqrt{2}}{2}$, D_{CA} is not the smallest Euclidean distance and P_{CA} no longer dominates the system performance, so we have

$$\int_0^\infty \int_{\sqrt{2}/2}^\infty f(H_b, \delta_2) \text{PDF}(\gamma) Q\left[\frac{H_b}{\sigma}\right] \text{d}H_b \text{d}\gamma < \text{RER}.$$

Thus, we have $\int_0^\infty f(H_b, \delta_2) Q[\frac{H_b}{\sigma}] \text{d}H_b < \text{RER}$. Note that for other BPSK-based HePNC, the above performance upper bound also holds. For higher-order modulation HePNC, the Euclidean distance between the BPSK circles D_{CA} no longer dominates the system performance when $\gamma < \frac{\sqrt{2}}{2}$. Thus, we can still obtain the same conclusion by the above analysis.

VI. Performance Evaluation

In this section, the performance of HePNC in asymmetric TWRC is evaluated. In the simulations, the relay is located on the line segment between the two sources. We let all nodes transmit signals with the same symbol energy E_s and set the average received SNR of all links be proportional to $d^{-\alpha}$, where d is the link distance and the path loss exponent $\alpha = 3$. Phase shift difference θ is uniformly distributed between $[0, 2\pi)$.

In the following, we first study the RER and the system BER_{all} performance of the proposed HePNC and JMR2 under both AWGN and Rayleigh fading channels, where JMR2 [27]

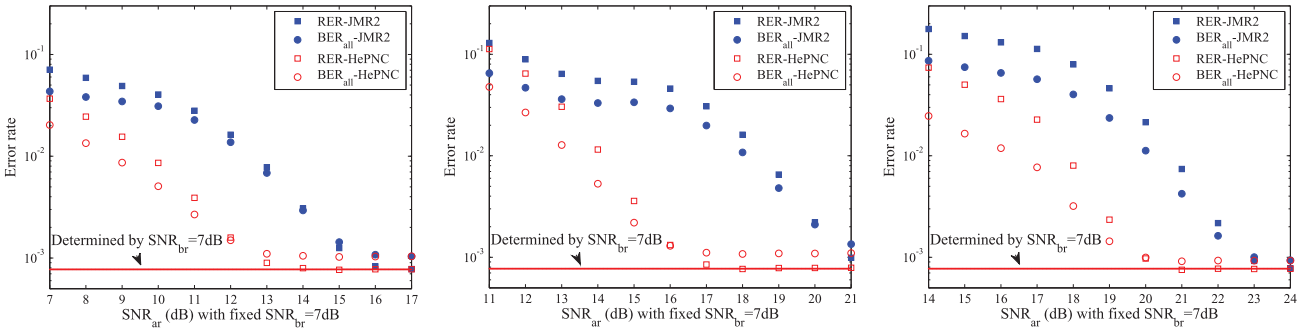

(a) QPSK-BPSK HePNC. (b) 8PSK-BPSK HePNC. (c) 16QAM-BPSK HePNC.

Fig. 9. Error rate with fixed SNR$_{br}$ in AWGN channels.

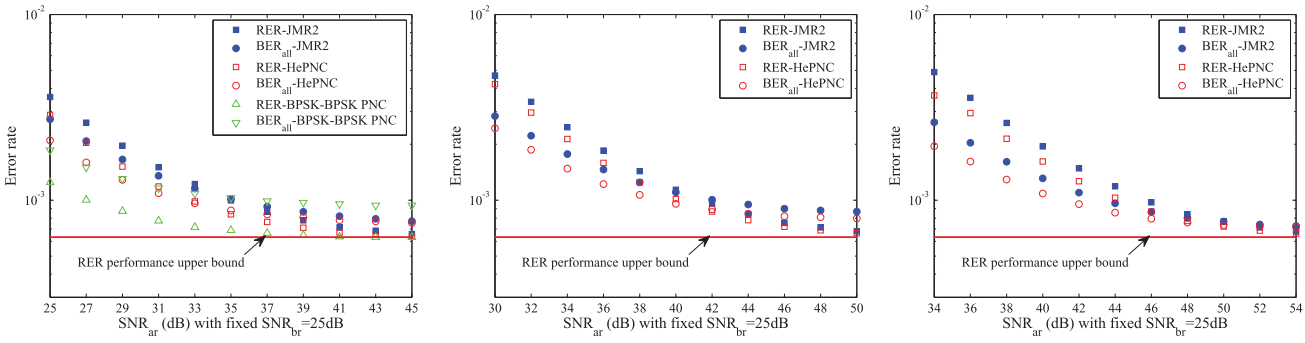

(a) QPSK-BPSK HePNC. (b) 8PSK-BPSK HePNC. (c) 16QAM-BPSK HePNC.

Fig. 10. Error rate with fixed SNR$_{br}$ in Rayleigh fading channels.

is the existing state-of-the-art solution, which does not use adaptive mapping. Then we study the optimal relay location issue. Further, we discuss how to maximize the throughput and minimize the energy consumption by jointly considering the modulation combination for the sources and the ratio of source data loads.

A. *Error Performance With Fixed SNR$_{br}$*

Fig. 9 compares the error performance of HePNC and JMR2 under AWGN channels, where we fix SNR$_{br}$ = 7 dB and gradually increase SNR$_{ar}$. Fig. 9(a) shows the error performance of QPSK-BPSK HePNC and QPSK-BPSK JMR2. For QPSK-BPSK HePNC, RER and BER$_{all}$ monotonously decrease with the increase of SNR$_{ar}$, and the RER performance converges to $Q[\sqrt{2 \cdot \text{SNR}_{br}}]$ as shown by the red solid line. For QPSK-BPSK JMR2, RER and BER$_{all}$ increase first and then decrease, because for different ΔSNR, the single mapping function may suffer a larger error probability for certain structures of the received constellation map. Adaptive mapping applied in HePNC can adjust the mapping functions suitable to the current received constellation map. From the figure, ensuring BER$_{all}$ below 10^{-3}, the proposed HePNC achieves 3 to 5 dB gain compared to JMR2. For the RER and BER$_{all}$ performance in QPSK-BPSK HePNC, when SNR$_{ar}$ is small, BER$_{all}$ is lower than RER; when SNR$_{ar}$ goes larger, RER is lower than BER$_{all}$. This is because when SNR$_{ar}$ is small, the BPSK circles on the received constellation map are relatively large, so the constellation points are close to or even overlap each other, which leads to a higher BER. When SNR$_{ar}$ is large, the BPSK circles are relatively small, and the errors that happen in the bottleneck link L_{br} dominate the performance of the BC stage.

Figs. 9(b) and 9(c) compare the performance of HePNC and JMR2 with 8PSK-BPSK and 16QAM-BPSK. For a higher-order modulation HePNC, a larger ΔSNR is needed to maintain the same BER and RER levels compared to the lower-order QPSK-BPSK HePNC. Given the same SNR$_{br}$, with the increase of SNR$_{ar}$, the RER performance of all the schemes converge to the error rate determined by $Q[\sqrt{2 \cdot \text{SNR}_{br}}]$, and BER$_{all}$ is bounded by (14); however, the HePNC schemes converge monotonously and more quickly than JMR2.

Fig. 10 shows the performance of HePNC and JMR2 under Rayleigh fading channels. We fix SNR$_{br}$ = 25 dB and gradually increase SNR$_{ar}$. When ΔSNR is large, the RERs of HePNC schemes converge to the error rate bounded by (16) as shown by the solid lines. However, HePNC does not have as high performance gain over JMR2 as that in the AWGN case. Because under the Rayleigh fading channels, $\gamma \in (0, \infty)$ with PDF(γ) is shown in (15). The channel condition of L_{ar} cannot be guaranteed always better than that of L_{br}, and the HePNC transmission may suffer a higher error rate for certain values of γ. Thus, if possible, the sources should apply adaptive modulation for HePNC according to the channel conditions. Fig. 10(a) also compares the error performance of QPSK-BPSK HePNC with BPSK-BPSK PNC. Under Rayleigh fading channel, the singular fade state affects the error performance of HePNC. Generally speaking, the error performance of higher-order modulation will result in worse error performance

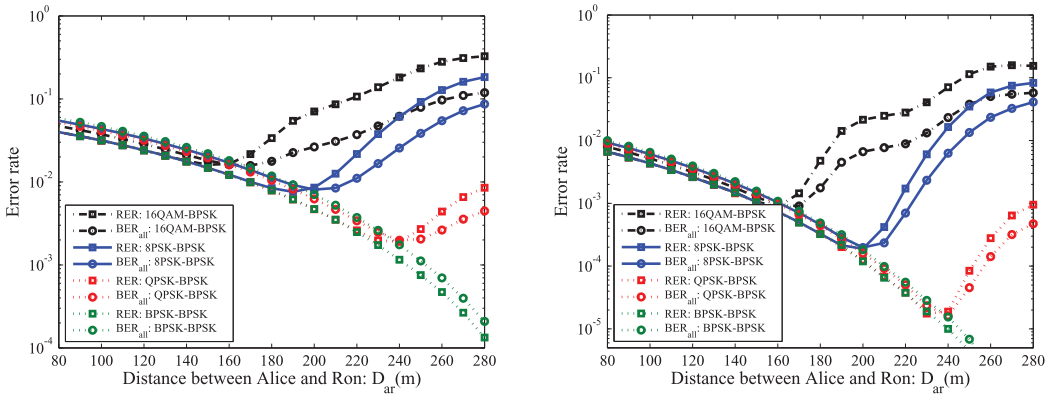

(a) $\mathrm{SNR}_{ab} = 0$ dB. (b) $\mathrm{SNR}_{ab} = 3$ dB.

Fig. 11. HePNC performance with fixed SNR_{ab}.

with the same value of SNR_{ar}. For example, when $\mathrm{SNR}_{ar} =$ 34dB, the BER for BPSK-BPSK converges to the minimum, around 0.001, while that for 16QAM-BPSK is around 0.002. Furthermore, when SNR_{ar} is large enough, the RER performance of BPSK-BPSK PNC and HePNC converge to the same value (determined by SNR_{br}) because the error performance is dominated by the errors happened within one BPSK circle. Note that the BER performance of HePNC is slightly better than BPSK-BPSK PNC in the higher SNR_{ar} region. This is because for HePNC, even the relay broadcasts an erroneous network-coded symbol, source node B still has a probability to correctly obtain a part of bits in the higher-order modulation symbols.

From Figs. 9 and 10, it is observed that a proper HePNC scheme should be selected according to the channel conditions of both the source-relay links. For example, in Fig. 9(a), SNR_{br} of the bottleneck link is 7dB, which can support the single hop BPSK modulation with BER less than 10^{-3} as shown by the solid line. However, if SNR_{ar} equals or is close to 7dB, the system BER performance of the QPSK-BPSK HePNC scheme is still much higher than 10^{-3}. Similar to the idea applied by the well known adaptive modulation, the HePNC system should consider both the two source-relay channel conditions and the data exchange ratio requirements to select the HePNC schemes. In Sec. VI-B, the suitable relay locations for different HePNC schemes will be obtained, and Sec. VI-C will study the throughput achieved for different data exchange ratio requirements.

B. Optimal Relay Issue With Fixed SNR_{ab}

We study how the relay's location influences the system error performance in a TWRC scenario where the relay is located on the line segment between the two sources. We fixed the distance between Alice and Bob as 600m. Denote the distance between Alice and Ron as D_{ar}, and we gradually increase D_{ar} by moving the relay from Alice towards Bob. Here, all channels are assumed AWGN ones. Note that, different from the scenario in Sec. VI-A, where error performance is studied by fixing SNR_{br}, here with the increase of D_{ar} by given SNR_{ab}, SNR_{ar} is smoothly reduced and SNR_{br} is smoothly increased.

Figs. 11(a) and 11(b) show the HePNC error performance with fixed $\mathrm{SNR}_{ab} = 0$ dB and 3 dB, respectively. In Fig. 11(a), we consider BER_{all} as the system performance index, and there are optimal relay locations existing for QPSK-BPSK, 8PSK-BPSK and 16QAM-BPSK HePNC at $D_{ar} =$240m, 200m and 170m, respectively. To compare with the symmetric PNC scheme, the green curves show the performance of symmetric BPSK-BPSK PNC, for which the optimal relay locates in the middle of the sources i.e., $D_{ar} =$ 300m. Note that for 8PSK-BPSK and 16QAM-BPSK HePNC, RERs are minimized when $D_{ar} =$ 200m and 150m. Thus, at the optimal relay locations where the system performance is optimized in terms of BER_{all}, the RER performance may not be optimal. Before reaching the optimal relay locations, BER_{all} decreases first thanks to the improvement of the bottleneck link SNR_{br}. After the optimal relay location, BER_{all} becomes worse because SNR_{ar} cannot further support the higher-order modulation, and the BPSK circles become so large that they lead to more errors.

The underlying reason why the optimal relay locations exist can be observed from Fig. 1(b). D_{ar} determines the structure of the received constellation map at the relay, i.e., smaller D_{ar} leads to smaller BPSK circles, and larger D_{ar} leads to larger BPSK circles. When the BPSK circles are too small, the errors happened within one BPSK circle cause a worse RER performance; when the BPSK circles are too large, errors happened between different BPSK circles would cause a higher RER. Thus, there exists an optimal location of the relay to minimize the RER performance, which further affects the overall BER performance of the system. In summary, given the traffic load and the locations of the two source nodes, we can identify the optimal relay location and select the best relay. Then given the relay location and conditions of two source-relay channels, we can configure the modulation accordingly.

Comparing different HePNC schemes, the optimal relay locations of higher-order modulation HePNC have a smaller D_{ar} since a larger SNR_{ar} is needed to support the higher-order modulation. When D_{ar} is small, e.g., $D_{ar} \in$ (80m, 140m), the RER performance of different HePNC schemes including the symmetric BPSK-BPSK PNC scheme are the same, because RER is dominated by the bottleneck SNR_{br}, and it can be estimated by $Q[\sqrt{2 \cdot \mathrm{SNR}_{br}}]$. Thus, HePNC can support the

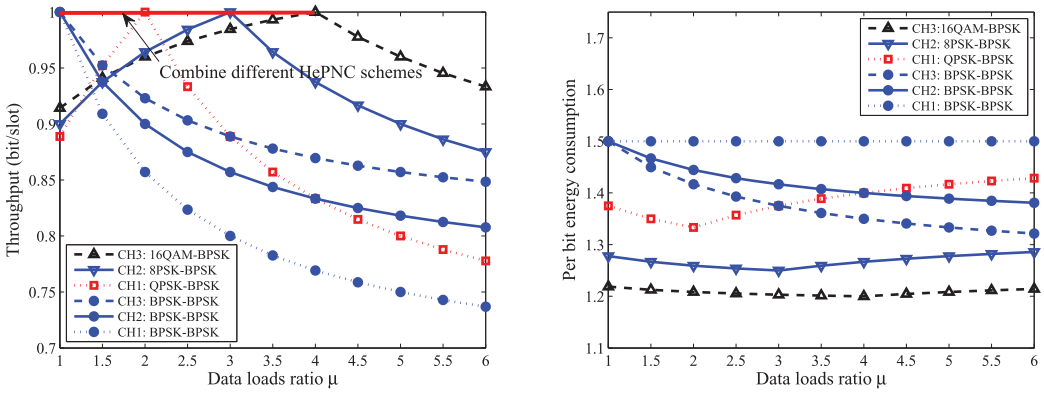

(a) Throughput upper bound. (b) Energy consumption.

Fig. 12. Throughput upper bound and energy efficiency.

asymmetric data exchange ratio[12] with the same error performance comparing to the symmetric BPSK-BPSK PNC scheme. BER_{all} of 8PSK-BPSK HePNC performs worst due to that the circle-shape constellation map has worse performance than the square-shape. 16QAM-BPSK HePNC performs best in terms of BER_{all} because more bits can be successfully exchanged when errors happen in the BC stage thanks to Gray mapping.

Fig. 11(b) shows the performance of different HePNC schemes with $\text{SNR}_{ab} = 3$ dB. The relay locations where RER and BER_{all} are minimized change slightly, and the overall error performance is improved. Considering BER_{all}, the optimal relay locations for QPSK-BPSK and 8PSK-BPSK HePNC remain the same. For 16QAM-BPSK HePNC, the optimal relay location changes to $D_{ar} = 160$m. Thus, to optimize the HePNC system, both of the MA and BC stages should be considered, as errors in the BC stage also affect the system performance.

C. Throughput and Energy Efficiency

In this section, the throughput upper bound and energy efficiency of HePNC and symmetric BPSK-BPSK PNC are studied and compared in an asymmetric TWRC scenario. We also consider asymmetric data loads of the sources. Let Sz_a denote the data load from Alice to Bob, and Sz_b vice versa. $\mu = Sz_a/Sz_b$ indicates the degree of traffic asymmetry. In addition, it is also assumed that the source node with the better link to the relay always has more data to send[13]. For simplicity, we define one slot equals the symbol duration. Note that, in the initialization of HePNC configuration, the relay needs to jointly consider the two source-relay channel conditions and the data exchange ratio requirements, which can be done by firstly transmitting requests from the sources to the relay individually including the data amount needed to be exchanged, and then the relay feedbacks the determined modulation scheme to the sources.

For a fair comparison, we consider three channel conditions: CH1, CH2 and CH3, in which link L_{ar} can support QPSK, 8PSK and 16QAM, respectively, with a negligible error rate, and link L_{br} can only support BPSK. In CH3, if not all the Alice's (or Bob's) bits can be transmitted by using the HePNC or BPSK-BPSK PNC scheme, the leftover bits are sent to Bob (Alice) through Ron in two hops using 16QAM and BPSK over L_{ar} and L_{br}, respectively. Similarly, L_{ar} is assumed to support up to QPSK and 8PSK for CH1 and CH2, respectively, with negligible error rates. Note that for the symmetric PNC, both source nodes can only use BPSK modulation due to the bottleneck link L_{br}.

Fig. 12(a) shows the throughput (bit/slot) upper bound of three HePNC schemes and the BPSK-BPSK PNC scheme under different traffic asymmetry μ. For BPSK-BPSK PNC, when $\mu = 1$, it achieves the highest throughput, 1 bit/slot; With the increase of μ, its throughput reduces, which indicates BPSK-BPSK PNC is not suitable to support the asymmetric data loads exchange. For the HePNC schemes, all the throughput curves increase first till reaching the maximum, 1 bit/slot, and then reduce to stable levels. QPSK-BPSK, 8PSK-BPSK and 16QAM-BPSK reach their maximum when $\mu = 2$, $\mu = 3$ and $\mu = 4$, respectively. This is because all the bits can be exchanged using HePNC with a high efficiency when μ equals the optimal value and no bit has to be sent using the two-hop relay path.

To generalize how to choose HePNC suitable to various μ, under the constraints of the channel quality, it is most desirable to use 2^{μ}-PSK or QAM and BPSK modulation scheme for Alice and Bob, respectively. While μ is a non-integer, hybrid HePNC with different modulations over the Alice–Ron link can be used. Assuming link L_{ar} can support $2^{\lceil\mu\rceil}$PSK–BPSK modulation (e.g., 16QAM), we can combine the HePNC using $2^{\lfloor\mu\rfloor}$PSK-BPSK and $2^{\lceil\mu\rceil}$PSK–BPSK to achieve the throughput of 1 bit/slot, e.g., when $\mu = 3.5$, 8PSK-BPSK HePNC and 16QAM-BPSK HePNC can be combined with a ratio of 1:1. Note that when both source-relay links can support 2^m-PSK or QAM (for $m > 1$), the throughput can be higher than 1 bit/slot.

In Fig. 12(b), the energy efficiency is evaluated in terms of per bit end-to-end energy consumption, which measures the average energy consumption for each bit being delivered from the source to the destination. In the simulation, the symbol energy is assumed to be a constant E_s. As shown in

[12]HePNC may support a higher throughput comparing to the symmetric PNC for the asymmetric data exchange ratio as discussed in Sec. VI-C.

[13]For example, L_{ar} has a higher average SNR than L_{br} and $\mu \geq 1$. For the case $\mu < 1$, HePNC can still be used but the throughput and energy gains over the existing PNC are not as obvious.

Fig. 12(b), HePNC also achieves a higher energy efficiency than PNC. Obviously, for different modulation combinations, the highest energy efficiency of HePNC is achieved when $\mu = \max(m_a, m_b)$, e.g., $\mu = 4$ for 16QAM-BPSK HePNC. One possibility to further improve the efficiency is to piggyback some bits from the relay node to the one with a better channel condition [42].

VII. Conclusion

In this paper, HePNC has been proposed to improve the efficiency in asymmetric TWRC scenarios, where the two source nodes have unbalanced traffic loads and their link conditions to the relay node are heterogeneous. We have investigated and presented three sample designs of HePNC, including QPSK-BPSK, 8PSK-BPSK and 16QAM-BPSK HePNC. We have introduced the HePNC design including how to optimize the many-to-one mapping and how to design the relay labeling process. The error performance of QPSK-BPSK HePNC has been analyzed under both AWGN and Rayleigh fading channels. The performance of HePNC system has been evaluated, and we obtained the optimal relay locations for the line topology. The throughput upper bound and energy efficiency analysis have demonstrated that HePNC can improve the spectrum and energy efficiency compared to the traditional homogeneous PNC schemes and the previous non-homogeneous scheme JMR2.

There are many open issues worth further investigation to fully understand the performance and application of HePNC. First, in a real network, fast fading may affect the HePNC's end-to-end BER performance as γ will change frequently, which may result in more frequent changes of the adaptive mapping functions and possibly more overheads. Second, although our proposed HePNC can enhance the throughput and energy efficiency compared to the symmetric PNC in asymmetric TWRC, multiple slots are needed to broadcast the network-coded symbol in the BC stage to guarantee the reliable transmission, which still limits the overall throughput of the HePNC schemes. How to effectively utilize the better link's transmission capacity in the BC stage is worth further research. One possible method is to apply the hierarchical modulation to piggyback bits on the network-coded symbol, which can achieve the bit transmissions from the relay to the source with the better source-relay channel condition in the BC stage. Third, the end-to-end channel coding can be integrated into HePNC naturally, and how to integrate the channel coding into the proposed HePNC in a link-to-link manner is still an open issue.

References

[1] H. Zhang, L. Zheng, and L. Cai, "HePNC: Design of physical layer network coding with heterogeneous modulations," in *Proc. IEEE Globecom*, 2014, pp. 2684–2689.

[2] S. Zhang, S. C. Liew, and P. P. Lam, "Hot topic: Physical-layer network coding," in *Proc. ACM MOBICOM*, 2006, pp. 358–365 .

[3] P. Popovski and H. Yomo, "The anti-packets can increase the achievable throughput of a wireless multi-hop network," in *Proc. IEEE Int. Conf. Commun. (ICC)*, 2006, pp. 3885–3890.

[4] T. Koike-Akino, P. Popovski, and V. Tarokh, "Optimized constellations for two-way wireless relaying with physical network coding," *IEEE J. Sel. Areas Commun.*, vol. 27, no. 5, pp. 773–787, Jun. 2009.

[5] V. Muralidharan, V. Namboodiri, and B. Rajan, "Wireless network-coded bidirectional relaying using Latin squares for M-PSK modulation," *IEEE Trans. Inf. Theory*, vol. 59, no. 10, pp. 6683–6711, Oct. 2013.

[6] R. Ahlswede, N. Cai, S.-Y. Li, and R. Yeung, "Network information flow," *IEEE Trans. Inf. Theory*, vol. 46, no. 4, pp. 1204–1216, Jul. 2000.

[7] S.-Y. R. Li, R. W. Yeung, and N. Cai, "Linear network coding," *IEEE Trans. Inf. Theory*, vol. 49, no. 2, pp. 1204–1216, Feb. 2003.

[8] S. C. Liew, S. Zhang, and L. Lu, "Physical-layer network coding: Tutorial, survey, and beyond," *Phys. Commun.*, vol. 6, pp. 4–42, Mar. 2013.

[9] S. Zhang, S. C. Liew, and L. Lu, "Physical layer network coding schemes over finite and infinite fields," in *Proc. IEEE Globecom*, 2008, pp. 1–6.

[10] B. Nazer and M. Gastpar, "Reliable physical layer network coding," *Proc. IEEE*, vol. 99, no. 3, pp. 438–460, Mar. 2011.

[11] D. K. S. Katti and S. S. Gollakota, "Embracing wireless interference: Analog network coding," in *Proc. ACM SIGCOMM*, 2007, pp. 397–408.

[12] L. Song, Y. Li, A. Huang, B. Jiao, and A. Vasilakos, "Differential modulation for bidirectional relaying with analog network coding," *IEEE Trans. Signal Process.*, vol. 58, no. 7, pp. 3933–3938, Jul. 2010.

[13] H.-M. Wang, X.-G. Xia, and Q. Yin, "A linear analog network coding for asynchronous two-way relay networks," *IEEE Trans. Wireless Commun.*, vol. 9, no. 12, pp. 3630–3637, Dec. 2010.

[14] S. Wang, Q. Song, X. Wang, and A. Jamalipour, "Rate and power adaptation for analog network coding," *IEEE Trans. Veh. Technol.*, vol. 60, no. 5, pp. 2302–2313, Jun. 2011.

[15] W. Nam, S.-Y. Chung, and Y. H. Lee, "Capacity of the Gaussian two-way relay channel to within 1/2 bit," *IEEE Trans. Inf. Theory*, vol. 56, no. 11, pp. 5488–5494, Nov. 2010.

[16] R. Knopp, "Two-way wireless communication via relay station," in *Proc. GDR-ISIS Meeting*, ENST, Paris, Mar. 2007.

[17] S. Katti, H. Rahul, W. Hu, D. Katabi, M. Medard, and J. Crowcroft, "XORs in the air: Practical wireless network coding," *IEEE/ACM Trans. Netw.*, vol. 16, no. 3, pp. 497–510, Jun. 2008.

[18] S. Zhang and S.-C. Liew, "Channel coding and decoding in a relay system operated with physical-layer network coding," *IEEE J. Sel. Areas Commun.*, vol. 27, no. 5, pp. 788–796, Jun. 2009.

[19] T. Huang, T. Yang, J. Yuan, and I. Land, "Design of irregular repeat-accumulate coded physical-layer network coding for Gaussian two-way relay channels," *IEEE Trans. Commun.*, vol. 61, no. 3, pp. 897–909, Mar. 2013.

[20] J. Li, J. Yuan, R. Malaney, M. Azmi, and M. Xiao, "Network coded LDPC code design for a multi-source relaying system," *IEEE Trans. Wireless Commun.*, vol. 10, no. 5, pp. 1538–1551, May 2011.

[21] R. Chang, S.-J. Lin, and W.-H. Chung, "Symbol and bit mapping optimization for physical-layer network coding with pulse amplitude modulation," *IEEE Trans. Wireless Commun.*, vol. 12, no. 8, pp. 3956–3967, Aug. 2013.

[22] M. Noori and M. Ardakani, "On symbol mapping for binary physical-layer network coding with PSK modulation," *IEEE Trans. Wireless Commun.*, vol. 11, no. 1, pp. 21–26, Jan. 2012.

[23] S. Wang, Z. Wen, Z. Meng, D. Chen, C. Li, and C. Fan, "Coordinated transceiver in MIMO heterogeneous network with physical-layer network coding," in *Proc. IEEE 24th Int. Symp. Pers. Indoor Mobile Radio Commun. (PIMRC)*, 2013, pp. 83–88.

[24] L. Bo, W. Gang, P. Chong, Y. Hongjuan, Y. Guan, and S. Xuejun, "Performance of physical-layer network coding in asymmetric two-way relay channels," *China Commun.*, vol. 10, no. 10, pp. 65–73, Oct. 2013.

[25] T. Koike-Akino, P. Popovski, and V. Tarokh, "Adaptive modulation and network coding with optimized precoding in two-way relaying," in *Proc. IEEE Globecom*, 2009, pp. 1–6.

[26] Z. Chen, H. Liu, and W. Wang, "A novel decoding-and-forward scheme with joint modulation for two-way relay channel," *IEEE Commun. Lett.*, vol. 14, no. 12, pp. 1149–1151, Dec. 2010.

[27] Z. Chen and H. Liu, "Spectrum-efficient coded modulation design for two-way relay channels," *IEEE J. Sel. Areas Commun.*, vol. 32, no. 2, pp. 251–263, Feb. 2014.

[28] B. Nazer and M. Gastpar, "Compute-and-forward: Harnessing interference through structured codes," *IEEE Trans. Inf. Theory*, vol. 57, no. 10, pp. 6463–6486, Oct. 2011.

[29] C. Feng, D. Silva, and F. Kschischang, "An algebraic approach to physical-layer network coding," *IEEE Trans. Inf. Theory*, vol. 59, no. 11, pp. 7576–7596, Nov. 2013.

[30] B. Hern and K. Narayanan, "Multilevel coding schemes for compute-and-forward," in *Proc. IEEE Int. Symp. Inf. Theory (ISIT)*, 2011, pp. 1713–1717.

[31] T. Yang and I. Collings, "On the optimal design and performance of linear physical-layer network coding for fading two-way relay channels," *IEEE Trans. Wireless Commun.*, vol. 13, no. 2, pp. 956–967, Feb. 2014.
[32] L. L. Shi L and Liew S C, "On the subtleties of q-PAM linear physical-layer network coding," arXiv preprint arXiv:1411, 2014.
[33] H. Zhang and L. Cai, "HePNC: A cross-layer design for MIMO networks with asymmetric two-way relay channel," in *Proc. IEEE Globecom*, 2015.
[34] J. He, P. Cheng, L. Shi, J. Chen, and Y. Sun, "Time synchronization in WSNs: A maximum-value-based consensus approach," *IEEE Trans. Autom. Control*, vol. 59, no. 3, pp. 660–675, Mar. 2014.
[35] S. Zhang, S.-C. Liew, and P. Lam, "On the synchronization of physical-layer network coding," in *Proc. IEEE Inf. Theory Workshop*, 2006, pp. 404–408.
[36] L. Lu, T. Wang, S. C. Liew, and S. Zhang, "Implementation of physical-layer network coding," in *Proc. IEEE Int. Conf. Commun. (ICC)*, 2012, pp. 404–408.
[37] Y. Huang, S. Wang, Q. Song, L. Guo, and A. Jamalipour, "Synchronous physical-layer network coding: A feasibility study," *IEEE Trans. Wireless Commun.*, vol. 12, no. 8, pp. 4048–4057, Aug. 2013.
[38] J. Craig, "A new, simple and exact result for calculating the probability of error for two-dimensional signal constellations," in *Proc. IEEE Mil. Commun. Conf. (MILCOM)*, 1991, pp. 571–575.
[39] X. Wang and L. Cai, "Proportional fair scheduling in hierarchical modulation aided wireless networks," *IEEE Trans. Wireless Commun.*, vol. 12, no. 4, pp. 1584–1593, Apr. 2013.
[40] Z. Yang, L. Cai, Y. Luo, and J. Pan, "Topology-aware modulation and error-correction coding for cooperative networks," *IEEE J. Sel. Areas Commun.*, vol. 30, no. 2, pp. 379–387, Feb. 2012.
[41] Z. Yang, Y. Luo, and L. Cai, "Network modulation: A new dimension to enhance wireless network performance," in *Proc. IEEE INFOCOM*, 2011, pp. 2786–2794.
[42] H. Zhang, L. Zheng, and L. Cai, "PiPNC: Piggybacking physical layer network coding for multihop wireless networks," in *Proc. IEEE Int. Conf. Commun. (ICC)*, 2015, pp. 6211–6216.

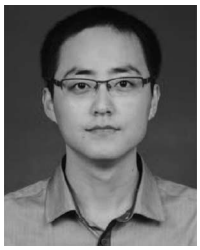

Haoyuan Zhang (S'14) received the B.S. and M.S. degrees in electrical and information engineering from Harbin Institute of Technology, Harbin, China, in 2010 and 2012, respectively. He is currently pursuing the Ph.D. degree in electrical and computer engineering at the University of Victoria, Victoria, BC, Canada. His research interests include error control channel coding, modulation optimizations, physical-layer network coding, and MIMO communications.

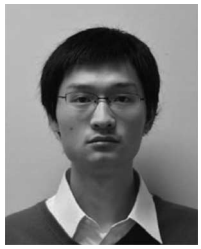

Lei Zheng (S'11) received B.S. and M.S. degrees in electrical engineering from Beijing University of Posts and Telecommunications, Beijing, China, and the Ph.D. degree from University of Victoria, Victoria, BC, Canada, in 2007, 2010, and 2015, respectively. His research interests include machine-to-machine networks, including medium access control protocol, radio resource allocation in wireless networks, and demand response control in smart grid.

Lin Cai (S'00–M'06–SM'10) received the M.A.Sc. and Ph.D. degrees in electrical and computer engineering from the University of Waterloo, Waterloo, Canada, in 2002 and 2005, respectively. Since 2005, she has been with the Department of Electrical and Computer Engineering, University of Victoria, Victoria, BC, USA, and she is currently a Professor. Her research interests include communications and networking, with a focus on network protocol and architecture design supporting emerging multimedia traffic over wireless, mobile, ad hoc, and sensor networks. She was a recipient of the NSERC Discovery Accelerator Supplement Grants in 2010 and 2015, and the best paper awards of the IEEE ICC 2008 and the IEEE WCNC 2011. She has served as a TPC symposium Co-Chair for the IEEE Globecom'10 and the Globecom'13, and an Associate Editor for the IEEE TRANSACTIONS ON WIRELESS COMMUNICATIONS, the IEEE TRANSACTIONS ON VEHICULAR TECHNOLOGY, *EURASIP Journal on Wireless Communications and Networking*, *International Journal of Sensor Networks*, and *Journal of Communications and Networks (JCN)*.